Supporting Information

Photoelectrochemical Behavior of n-Type Si(111) Electrodes Coated With a Single Layer of Graphene

Adam C. Nielander†, Matthew J. Bierman†, Nicholas Petrone‡, Nicholas C. Strandwitz†, Shane Ardo†, Fan Yang†, James Hone*‡, Nathan S. Lewis*,†

†Division of Chemistry and Chemical Engineering, California Institute of Technology, Pasadena, CA, 91125, United States

‡Department of Mechanical Engineering, Columbia University, New York, New York, 10027, United States

Methods

Chemicals/Materials

All experiments employed single-crystalline, Czochralski grown, (111)-oriented, planar, 380 μm thick, phosphorus doped, 1.1 Ω-cm resistivity (doping density, $N_D \approx 5x10^{15}$ cm^{-3}) n-type silicon (University Wafer).

Water was obtained from a Barnstead Nanopure system and had a resistivity ≥ 18.0 MΩ-cm. Copper Etch Type CE – 100 ($FeCl_3$-based, Transene Company, Inc., Danvers, MA), Copper Etch Type APS – 100 (Ammonium persulfate-based, Transene), buffered HF(aq) (semiconductor grade, Transene Company, Inc., Danvers, MA), and 11 M NH_4F(aq) (semiconductor grade, Transene) were used as received. Acetone (HPLC grade, Sigma-Aldrich) was used as received. Acetonitrile (99.8% anhydrous, Sigma-Aldrich) that was used in electrochemical measurements was dried over Al_2O_3 prior to use.

Ferrocene (Fc, bis(cyclopentadienyl)iron(II), 99%,Strem), cobaltocene ($CoCp_2$, bis(cyclopentadienyl)cobalt(II), 98%, Strem), and acetylferrocene (AcFc, (acetylcyclopentadienyl)-cyclopentadienyl iron(II), 99.5%, Strem) were purified via sublimation. Ferrocenium tetraflouroborate ($Fc^+[BF_4]^-$, bis(cyclopentadienyl)iron(III) tetraflouroborate, technical grade, Sigma-Aldrich) was recrystallized from a mixture of diethyl ether (ACS grade, EMD) and acetonitrile (ACS grade, EMD) and dried under vacuum. Cobaltocenium hexafluorophosphate ($CoCp_2^+$, bis(cyclopentadienyl)cobalt(III) hexafluorophosphate, 98%, Sigma-Aldrich) was recrystallized from a mixture of ethanol (ACS grade, EMD) and acetonitrile (ACS grade, EMD) and dried under vacuum. Acetylferrocenium ($AcFc^+$) was

generated in situ via electrochemical oxidation of AcFc with the concomitant reduction reaction occurring in a compartment separated from the electrochemical cell using a Vycor frit.

Potassium ferricyanide ($K_3[Fe(CN)_6]$, 99.2%, Sigma-Aldrich) and potassium ferrocyanide ($K_4[Fe(CN)_6]\cdot 3H_2O$, ACS Certified, Fischer Scientific) were used as received. $LiClO_4$ (battery grade, Sigma-Aldrich) was used as received. Petri dishes used were Falcon Optilux™ branded and were cleaned with water prior to use. All other chemicals were used as received unless otherwise noted.

Electrode Fabrication

A monolayer film of graphene was formed via chemical-vapor deposition (CVD) of carbon onto a Cu foil. A 25 μm-thick Cu foil (99.999%, Alfa Aesar) was heated in a tube furnace to 800 °C at a pressure of 50 mTorr and annealed for 10 h under a 2 sccm flow of H_2(g). Graphene was subsequently synthesized on the surface of the copper foil by flowing CH_4(g) (35 sccm) and H_2(g) (2 sccm) at 1000 °C and 250 mTorr. This method of graphene growth has been shown to grow polycrystalline, monolayer graphene and Figure S1 shows a representative Raman spectrum of the starting material graphene on 300 nm SiO_2 on Si.[1] After growth of the graphene, the gas flow rates and chamber pressure were maintained and the Cu foil was rapidly cooled to room temperature by removing the furnace from the growth section of the process tube. The graphene synthesis resulted in grains that were 0.2 to 5 μm on a side, and an analysis of the grain size and grain distribution of the resulting polycrystalline graphene film has been presented in Petrone, et al., 2008.[1] The surface was then covered with a coating of 495K A4 polymethyl methacrylate (PMMA, MicroChem) by spinning at 2000 RPM (500 RPM s^{-1} acceleration) for 60 s, followed by a 10 10-min bake at 185 ˚C. This procedure was repeated for a total of two PMMA applications. The Cu was etched away using either a 15% (v:v) $NH_4(S_2O_8)_2$ (aq) solution or a 40% $FeCl_3$/1% HCl(aq) solution (Transene).[2] Cu removal was determined visually and confirmed by XPS analysis (Figure S6). To remove etchant residue, the resultant PMMA/graphene stack was transferred consecutively to three fresh baths of 18 MΩ-cm resistivity H_2O in petri dishes. The transfer was executed using a freshly piranha-cleaned (7:3 H_2SO_4:H_2O_2, aqueous solution) SiO_2-coated Si wafer to collect the PMMA/Gr stack from one bath and release the stack in a fresh H_2O bath. N-type Si samples were washed consecutively with H_2O, methanol,

acetone, methanol, and H_2O, and were then submerged in a piranha solution for 10 min and etched for 30 s in buffered HF(aq). The cleaned PMMA/graphene stack was transferred from a water bath to the cleaned, freshly HF(aq) etched Si(111) surface, and a gentle stream of N_2(g) was used to remove H_2O from the intervening space between the graphene and the Si. The PMMA/graphene/Si stack was then heated at 80 °C for 10 min in air, followed by submersion for 10 min in acetone to remove the PMMA layer. The resulting Si/graphene (Si/Gr) stack was annealed for ~8 h at 300 °C under forming gas (95:5 v:v N_2:H_2) to further remove PMMA residue from the surface of the graphene.[1] Si/Gr electrodes ~ 0.02 cm^2 in area were then fabricated with the use of GaIn (75:25 mass:mass) eutectic as a back ohmic contact. The electrodes were affixed to a Cu wire with Ag paint, and all surfaces, except the electrode, were insulated from the electrolyte by use of Loctite Hysol 9460 epoxy. On average, out of ten fabricated electrodes, two to three showed very low shunt resistances in nonaqueous electrolytes and/or displayed minimal protection of the Si surface from oxidation. The remaining 7-8 electrodes gave data consistent with that shown Figures 1, 2, and 3. An analogous process was used to fabricate electrodes that were not coated with graphene (n-Si–H and n-Si–Me electrodes). Methylated silicon wafers were prepared using a previously reported procedure.[3] Before use, the graphene-free, non-methylated Si electrodes were terminated with Si-H bonds by exposure to buffered HF(aq) for 30 seconds. Electrodes were also fabricated by exposing silicon wafers to the same conditions as the graphene-transfer procedure, except that no graphene was present between the PMMA and Cu. Such electrodes were not HF-etched prior to use.

Instrumentation

X-ray photoelectron spectroscopy (XPS) data was collected at ~5×10^{-9} Torr using a Kratos AXIS Ultra DLD with a magnetic immersion lens that consisted of a spherical mirror and concentric hemispherical analyzers with a delay-line detector (DLD). An Al Kα (1.486 KeV) monochromatic source was used for X-ray excitation. Ejected electrons were collected at an angle of 90° from the horizontal. The CASA XPS software package v 2.3.16 was used to analyze the collected data.

Electrochemical data were obtained using a Princeton Applied Research Model 2273 or a Gamry Reference 600 potentiostat. A Pt wire reference electrode (0.5 mm dia., 99.99% trace metals basis, Sigma-Aldrich) and a Pt mesh counter electrode (100 mesh, 99.9% trace metals basis, Sigma-Aldrich) were used for the electrochemical measurements. The cell potentials for the nonaqueous redox species were determined using cyclic voltammetry to compare the solution potential to the formal potential of the redox species. The potential difference between cells was calculated using the difference between the formal potentials for each redox couple using standard potentials from the literature.[4] The CH_3CN-$CoCp_2^{+/0}$ solution ($CoCp_2$ [3 mM]/ $CoCp_2^+$ [50 mM]) was calculated to have a solution potential of -1.26 V vs Fc/Fc^+, the CH_3CN-$Fc^{+/0}$ solution (Fc [55 mM]/ Fc^+ [3 mM]) was calculated to have a solution potential of -0.10 V vs Fc/Fc^+, and the CH_3CN-$AcFc^{+/0}$ solution (pre-electrolysis AcFc concentration = [50 mM]) was calculated to have a solution potential of +0.40 V vs Fc/Fc^+. The nonaqueous electrochemical solutions each contained 1.0 M $LiClO_4$. The aqueous $K_3[Fe(CN)_6]/K_4[Fe(CN)_6]$ ($[Fe(CN)_6]^{-3}$, 50mM; $[Fe(CN)_6]^{-4}$, 350mM) solution contained no additional supporting electrolyte due to the high intrinsic salt concentration. The current under forward bias saturated at much larger values in the $Fe(CN)_6^{3-/4-}$ solution relative to in the Fc^+/Fc solution because of the increased concentration of electron-accepting species in the $Fe(CN)_6^{3-/4-}$ solution. CH_3CN-$Fc[BF_4]$ is a highly colored species that at high concentrations absorbs a significant fraction of the light prior to photons striking the photoelectrode. The electrolyte solution was rapidly stirred with a small, Teflon-covered stir bar. Illumination was provided with an ELH-type tungsten-halogen lamp. Illumination intensities were set to provide either 3-5 mA cm^{-2} or ~10-11 mA cm^{-2}. These values corresponded to ~1/10th and ~1/3rd of a Sun (~10 mW cm^{-2} and ~33 mW cm^{-2}), respectively, as determined through the concurrent use of a Si photodiode (Thor Laboratories) that was calibrated relative to a secondary standard photodetector that was NIST-traceable and calibrated at 100 mW cm^{-2} of AM1.5 illumination. Nonaqueous electrochemistry was performed anaerobically in an Ar(g)-filled glovebox. Aqueous electrochemistry was performed in air. Electrodes were washed with H_2O and isopropanol and dried prior transfer between electrolyte solutions.

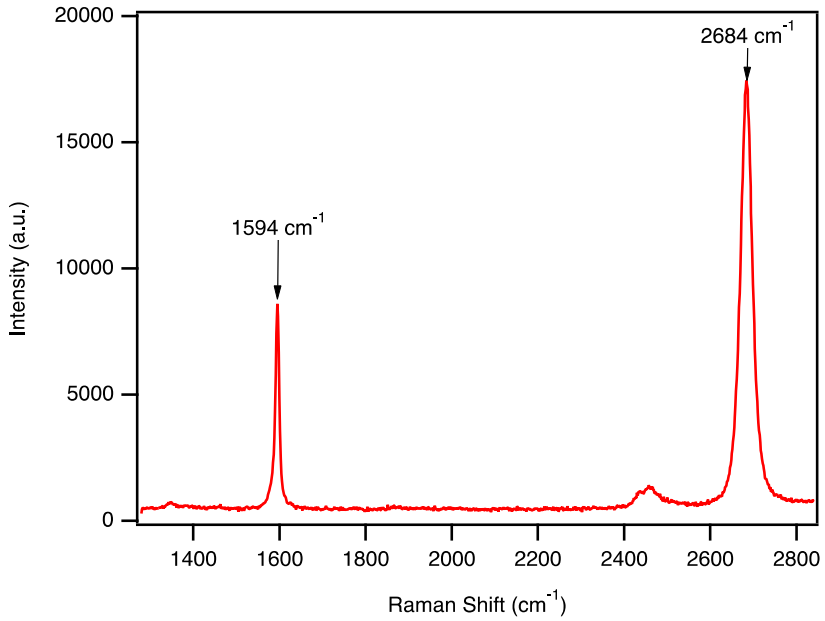

Figure S1. Representative Raman spectrum of starting material graphene on 300 nm SiO_2 (λ=532 nm). Sharp G (1594 cm^{-1}, FWHM: 10 cm^{-1}) and 2D peaks (2684 $cm^{-1,}$ FWHM: 32 cm^{-1}), as well as a small defect peak (~1350 cm^{-1}) confirm the monolayer, defect-free nature of the starting material.[5,6]

Mott-Schottky Fitting Procedure

To perform the Mott-Schottky analysis, a 10 mV sinusoidal AC signal was superimposed over DC biases of 0.30, 0.35, 0.4, 0.45, 0.50, 0.55, and 0.60 V versus the Nernstian potential of the solution. The frequency of the AC signal was varied from 50 to 300 kHz at each DC bias. The impedance data were modeled by the equivalent Randle's circuit shown in figure S2, and best fits were obtained using the fitting procedure executed by the ZView electrochemical software (Scribner Associates, Inc.). The data in Table S1 and Table S2 were used to approximate the area-normalized series resistance imparted to the n-Si/Gr electrodes by the fabrication procedure at approximately 9 Ω cm^2 by comparing the average area-normalized resistance of the n-Si/Gr and n-Si–H electrodes (24.4 Ω cm^2 and 15.1 Ω cm^2, respectively). The *J-E* data of n-Si/Gr under illumination in contact with CH_3CN-$Fc^{0/+}$ electrolyte indicated a series resistance of 23.1 ± 5.1 Ω cm^2 (6 electrodes), in excellent accord with data found via electrochemical impedance spectroscopy.

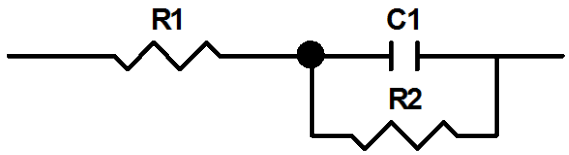

Figure S2. Equivalent circuit used to analyze the impedance data.

Voltage (V)	R1(Ω cm^2)	R2(Ω cm^2)	C1 (μF cm^{-2})
0.25	25.6	7656.2	2.89E-02
0.3	24.7	7685.7	2.73E-02
0.35	23.9	7641.1	2.62E-02
0.4	24.3	7642.4	2.53E-02
0.45	24.4	7577.3	2.47E-02
0.5	24.2	7615.4	2.39E-02
0.55	24.2	7661.3	2.33E-02
0.6	24.1	7688.3	2.27E-02

Table S1. Results obtained from the fitting of the impedance data at each applied voltage for the representative n-Si/Gr electrode.

Voltage (V)	R1(Ω cm^2)	R2(Ω cm^2)	C1 (μF cm^{-2})
0.25	12.9	154180.5	4.07E-03
0.3	13.7	95594.4	3.99E-03
0.35	14.2	84057.0	3.91E-03
0.4	15.0	60479.1	3.83E-03
0.45	15.5	49401.7	3.74E-03
0.5	16.1	47259.1	3.67E-03
0.55	16.7	49229.5	3.60E-03
0.6	17.4	41858.1	3.54E-03

Table S2. Results obtained from the fitting of the impedance data at each applied voltage for the representative n-Si–H electrode.

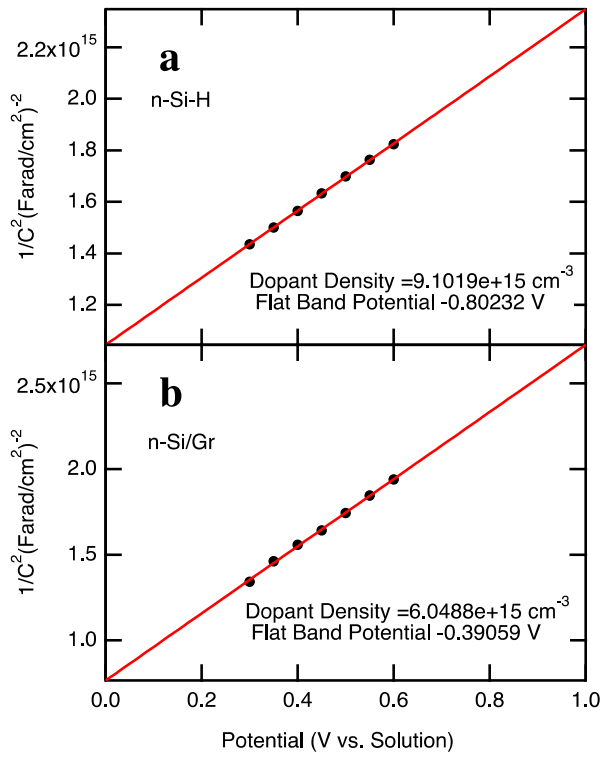

Figure S3. Mott-Schottky (C_{diff}^{-2} vs E) behavior of (a) n-Si–H and (b) n-Si/Gr electrodes in contact with CH_3CN-$Fc^{+/0}$ in the dark. The differential capacitance (C_{diff}) at each voltage was determined by fitting the impedance vs. frequency data between 50 kHz and 300 kHz to an equivalent Randle's circuit at each voltage. The doping density measured by 4-point probe technique was calculated to be N_D~5x10^{15} cm^{-3}.

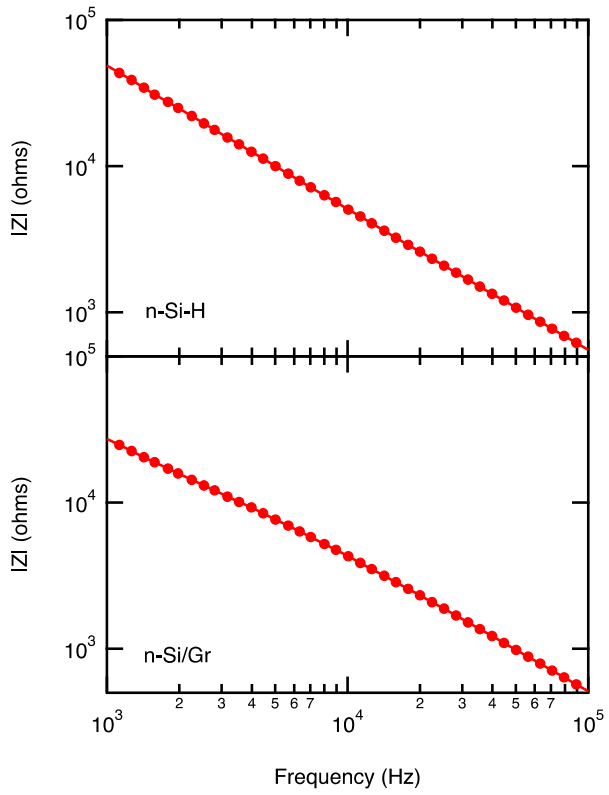

Figure S3. Bode plot of n-Si–H and n-Si/Gr electrodes in contact with CH_3CN-$Fc^{+/0}$ in the absence of illumination at E = 0.40 V vs. the Nernst potential of the solution.

Description of Semiconductor/Gr/Electrolyte Model

To gain a better understanding of the electrochemical and photoelectrochemical effects of graphene, the equilibration of the three-phase semiconductor/graphene/electrolyte system was analyzed. The following assumptions were made:

- The Fermi level of all three phases is the same at equilibrium.
- Equilibrium is obtained through charge transfer between the three phases.
- The initial Fermi level of the semiconductor ($E_{F,SC}$) is closer to the vacuum level than the initial Fermi level of graphene ($E_{F,Gr}$), which is in turn is closer to the vacuum level than the initial Fermi level of the electrolyte ($E_{F,electrolyte}$).

- The sum of the net charge in the three phases is zero, as required by electroneutrality: $Q_{sc} + Q_{Gr} + Q_{liquid} = 0$, where Q_{sc} is the net charge in the semiconductor, Q_{Gr} is the net charge in the graphene, and $Q_{electrolyte}$ is the net charge in the liquid electrolyte.
- The potential drop in the semiconductor (V_{bi}) is well-modeled by the potential drop of a semiconductor under depletion conditions.
- The potential drop in the electrolyte (V_H) is well-modeled using the known capacitive and dielectric properties of a typical electrolyte solution.
- The Fermi level of the graphene phase may be strongly shifted by the addition or loss of electrons, due to the low density of states and atomically thin structure of the graphene. This shift (V_{Gr}) can be predicted using the theoretically calculated DOS of graphene.[7] V_{Gr} is a shift in the graphene Fermi level and not an electrostatic potential drop.
- The potential drop in the interfacial layer between the semiconductor and graphene, as well as the potential drop the interfacial layer between graphene and the liquid electrolyte contact, is negligible.

Essentially, Poisson's equation was solved while treating the n-Si/Gr/electrolyte interface as consisting of a depleted semiconductor (Si) of known dielectric and capacitive properties in contact with an atomically thin material with the known density of electronic states as a function of energy of graphene, with this entire phase in contact with a phase consisting of the known dielectric and capacitive properties representative of a typical electrolyte solution. This treatment parallels, and is consistent with, the interfacial charge equilibration and surface state models that have been developed previously for semiconductor surfaces and are extensively described in the literature.[8,9] To calculate the equilibrium values of Q_{sc}, Q_{Gr}, and $Q_{electrolyte}$, as well as V_{bi} and V_H, the analysis was broken down into two steps and iterated. First, the equilibrium values for the two-phase Gr/electrolyte system were determined using Poisson's equation. Then, using these values as the starting condition, the final self-consistent state for

the two-phase Si/Gr system was solved using Poisson's equation. These values were then used as starting conditions for the first two-phase Gr/electrolyte system, and the process was iterated until the values converged to a global minimum. Poisson's equation was solved using a method previously described for equilibration of a two-phase system.[8]

The constants used in the modeling were as follows. The electron affinity of Si was taken to be -4.05 eV vs. vacuum.[10] The Fermi level of phosphorous-doped Si (N_D= 10^{15} cm^{-3}) was calculated to be ~ -4.3 eV. The intrinsic Fermi level of graphene was taken to be -4.6 eV vs. vacuum.[11] The empirical built-in potential difference in the absence of graphene (V_{bi} = 0.8 V) was used to calculate the Fermi level of the liquid electrolyte contacting phase, qE(A/A$^-$) = -5.1 eV versus vacuum (Figure S3). The DOS of graphene is known,[7] and from this, [d(DOS)/d$E_{F, Gr}$] was taken to be 1.5x10^{-5} C/eV. The thickness of the Helmholtz layer was set to 5x10^{-8} cm and κ_l was set to 4.0.[12,13]

The potential distribution in the two-phase Gr/electrolyte system was modeled by the following equations:

$$\phi_{Gr} - \phi_{Electrolyte} = V_{Gr} + V_H \qquad (1)$$

where ϕ_{Gr} is the Fermi level of the graphene with respect to vacuum, $\phi_{electrolyte}$ is the Fermi level of the liquid electrolyte with respect to vacuum,

$$V_{Gr} = \pm\sqrt{\frac{|Q_{Gr}+\Delta Q|}{0.5*\frac{dDOS}{dE_{F,Gr}}}} \qquad (2)$$

and

$$V_H = \frac{D*|Q_{Electrolyte}+\Delta Q|}{\varepsilon_0*\kappa_l} \qquad (3)$$

where Q_{Gr} = $Q_{electrolyte}$ = 0, ΔQ is the change in charge required to reach equilibrium, [d(DOS_{Gr})/d$E_{F, Gr}$] is determined from the reported DOS of graphene with respect to $E_{F, Gr}$, D is the thickness of the Helmholtz layer, ε_o is the permittivity of free space, and κ_l is the relative permittivity of the liquid phase.[7] The solution to this system of equations results in two values for ΔQ because of its quadratic dependence; however, only one of the results is physical. The equilibrium charge distributions for the two-phase

Gr/liquid system are $Q_{\text{Gr, eq-a}} = \Delta Q$ and $Q_{\text{electrolyte, eq}} = -\Delta Q$. The energy of the Fermi levels at equilibrium implies that the graphene is positively charged and the liquid phase is negatively charged.

To determine the charge distribution for the three-phase Si/Gr/electrolyte system, the two-phase Si/Gr system was modeled by the following equation:

$$\phi_{sc} - \phi_{Gr} = V_{bi} - V_{Gr} \tag{4}$$

where:

$$V_{bi} = \frac{(Q_{sc} + \Delta Q)^2}{2qN_D\varepsilon_0\kappa_{sc}} \tag{5}$$

and

$$V_{Gr} = \pm\sqrt{\frac{|Q_{Gr} - \Delta Q|}{0.5 * \frac{dDOS}{dE_{F,Gr}}}} \tag{6}$$

where $Q_{sc} = 0$, $Q_{Gr} = Q_{\text{Gr, eq-a}}$ from above, ΔQ is the change in charge required to reach equilibrium, q is the elementary charge, N_D is the dopant density, ε_o is the permittivity of free space, and κ_{sc} is the relative permittivity of the semiconductor phase.[8] The sign convention on ΔQ was chosen to reflect the decrease in positive charge on the graphene phase and the increase in positive charge on the semiconductor. The graphene phase "loses" charge because it was previously positively charged from equilibration with the liquid phase, and the relative Fermi levels of the semiconductor and graphene phases dictate that the semiconductor transfers negative charge to the graphene. The solution to this system of equations results in four values for ΔQ because of its quartic dependence; however, only one of the results is physical. The equilibrium charge distributions for the two-phase Si/Gr system are $Q_{\text{sc, eq}} = \Delta Q$ and $Q_{\text{Gr, eq-b}} = (Q_{\text{Gr, eq-a}} - \Delta Q)$. The energy of the Fermi levels at equilibrium implies that the semiconductor is positively charged and that the graphene remains positively charged.

Equilibration of the two-phase Si/Gr system resulted in non-equilibrium conditions for the two-phase Gr/liquid system as the graphene charge density, and thus potential drop, changed. Thus, the first set of equations was re-solved with the initial conditions, $Q_{\text{Gr}} = Q_{\text{Gr, eq-b}}$ and $Q_{\text{electrolyte}} = Q_{\text{electrolyte, eq}}$. The

solutions were then used as initial conditions in the second set of equations as $Q_{sc} = Q_{sc}$, eq and $Q_{Gr} = Q_{Gr,\ eq\text{-}a}$, re-solved, and the process was iterated until $|Q_{Gr,\ eq\text{-}a} - Q_{Gr,\ eq\text{-}b}| < Q_{Gr,\ eq\text{-}a} \times 10^{-5}$. The converged values of the charges were determined to be $Q_{sc,\ eq} = (+)\ 2.30 \times 10^{-8}$ C, $Q_{Gr,\ eq\text{-}a} = Q_{Gr,\ eq\text{-}b} = (+)\ 9.67 \times 10^{-7}$ C, and $Q_{electrolyte,\ eq} = (-)\ 9.97 \times 10^{-7}$ C. These were used to calculate the potential drops: $V_{bi} \approx 0.65$ V, $V_{Gr} \approx 0.35$ and $V_H \approx 0.15$ V. For comparison, for the two-phase Si/liquid electrolyte system $Q_{sc,\ eq} = (+)\ 1.64 \times 10^{-8}$ C, $Q_{electrolyte,\ eq} = (-)\ 1.64 \times 10^{-8}$ C, $V_{bi} = 0.797$ V, and $V_H = 0.0030$ V. These trends are consistent with the experimentally observed V_{oc} values (Figure 1).

XPS Analysis

XPS analysis was performed in order to determine the effect of graphene-covering procedure on the n-Si surface. No silicon oxide was detected on freshly HF-etched silicon surfaces (Figure S4). Silicon oxide was detected on the graphene-covered sample (Figure S5) and quantified using a simple substrate—overlayer model described by equation 7[14]:

$$d = \lambda_{ov} \sin\theta \left\{ \ln\left[1 + \frac{I_{Si}^{o}}{I_{ov}^{o}} * \frac{I_{ov}}{I_{Si}} \right] \right\} \qquad (7)$$

Where d is the overlayer thickness, λ_{ov} is the attenuation factor through the oxide overlayer (assumed to be 2.6 nm)[15], θ the angle from the surface of the sample to the detector (90°), $\frac{I_{Si}^{o}}{I_{ov}^{o}}$ is an instrument normalization factor related to the expected signal for a pure Si and a pure SiO_2 sample (taken to be 1.3 for this instrument), I_{ov} is the measured intensity of the silicon, and I_{ov} is the measured intensity of the silicon oxide overlayer. The thickness of a monolayer of oxide was taken to be 0.35 nm.[16] Using the data in figure S5, equation 7 indicates that the oxide thickness was approximately 0.41 nm, or 1-2 monolayers of oxide.

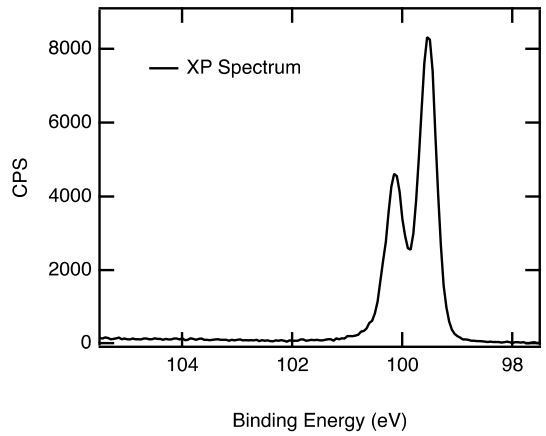

Figure S4. Representative high resolution XP spectrum of the Si 2p region of a silicon wafer that had been etched in HF (aq) just prior to XPS analysis. The lack of a peak in the 102-104 eV region indicates that there was not silicon oxide present at the Si surface prior to covering the wafer with graphene.

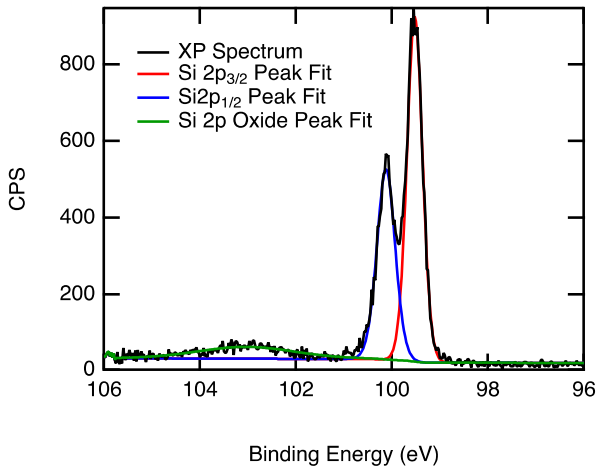

Figure S5. Representative high resolution XP spectrum of the Si 2p region of a silicon wafer covered by graphene. Peak fitting gave peak areas of 80, 239, and 369 for the SiOx, Si $2p_{½}$ and Si $2p_{3/2}$ peaks, respectively.

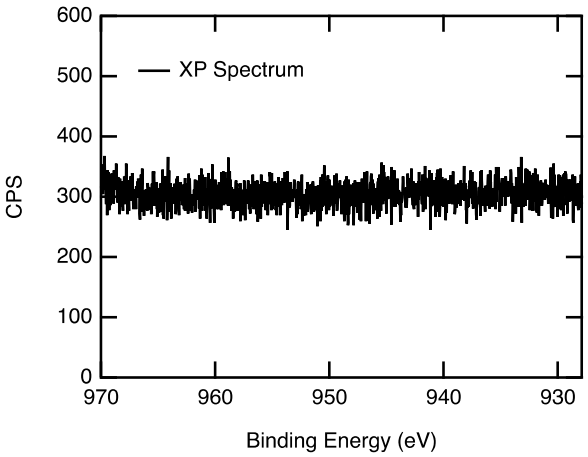

Figure S6. Representative high resolution XP spectrum of the copper region of a silicon wafer covered by graphene. Spectrum indicated copper impurities below the detection limit of the XPS instrument used.

Methylated n-Si stability versus graphene-covered n-Si stability

It is interesting to compare the electrochemical stability imparted by the presence of a graphene layer to the stability imparted by methyl-termination of the silicon surface since both entail a single layer of carbon atoms covering a silicon lattice. As seen in figure S7, at lower light intensities, the n-Si-Me electrode performance is comparable to that of the n-Si/Gr electrode performance. However, as seen in figure S8, at higher light intensities, the n-Si/Gr electrode yielded more stable performance than the n-Si-Me electrode. Future studies will evaluate the stability when these protection techniques are used in tandem.

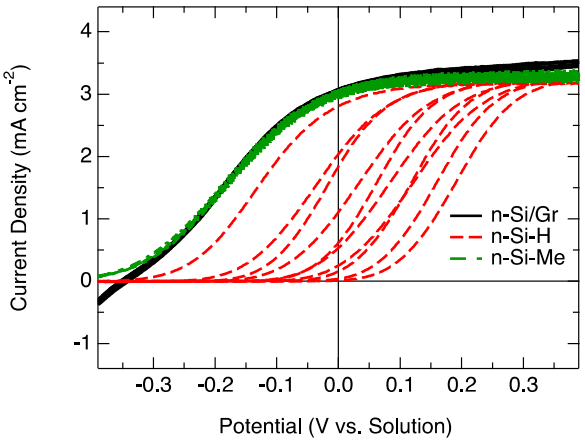

Figure S7. *J-E* behavior (5 cycles at 30 mV s^{-1}) of the n-Si/Gr, n-Si-Me and n-Si-H electrodes $Fe(CN)_6^{3-/4-}$(aq) under ELH lamp illumination necessary to give ~3 mA cm^{-2} light-limited current density.

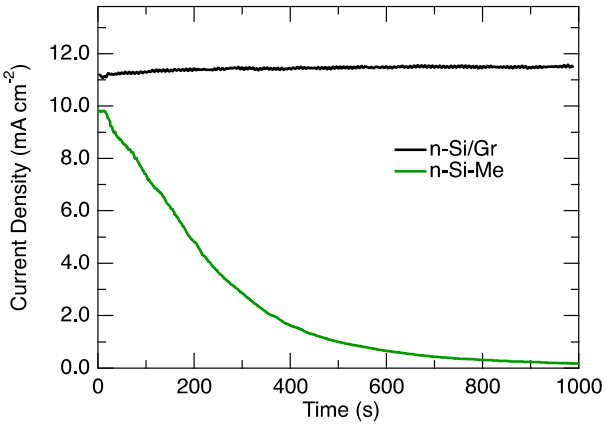

Figure S8. *J–t* behavior of an n-Si/Gr and a n-Si-Me electrode in $Fe(CN)_6^{3-/4-}$(aq) under illumination required to produce a short-circuit photocurrent density of 10-11 mA cm^{-2} over 1000 s (E = 0 V vs. solution).

PMMA/Cu Control electrodes

Bare n-Si electrodes were fabricated analogously to graphene-covered electrodes except that PMMA/Cu stacks were used instead of PMMA/Gr/Cu stacks. As shown in Figure S9, such PMMA/Cu

coated Si electrodes were unstable under our test conditions and exhibited rapid passivation due to oxide formation.

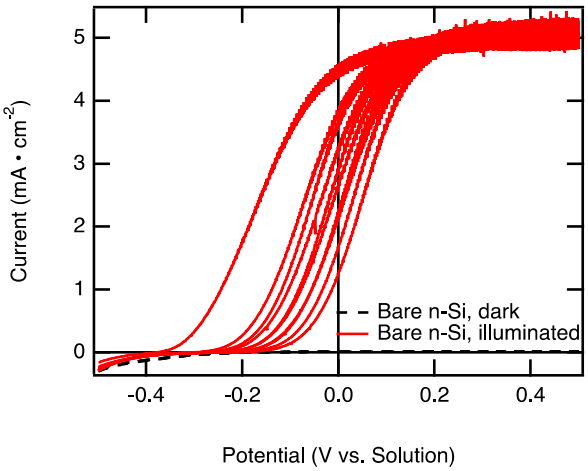

Figure S9. *J-E* behavior (5 cycles at 50 mV s^{-1}) of a bare n-Si electrode exposed to the graphene transfer procedure in $Fe(CN)_6^{3-/4-}$(aq) under approximately $1/10^{th}$ sun illumination provided by an ELH lamp.

n-Si/Gr and n-Si–H Electrode stability at ~100 mW cm^{-2}

As seen in Figure S10, both the n-Si/Gr and n-Si–H electrodes showed degradation of performance under approximately 1 sun illumination, albeit at reduced rates for the n-Si/Gr electrode. This underscores the need for further strategies, such as methyl termination combined with graphene multiple layers of graphene, in order to address the challenging issue of obtaining long-term protection of Si in aqueous solution while evolving oxygen from water.

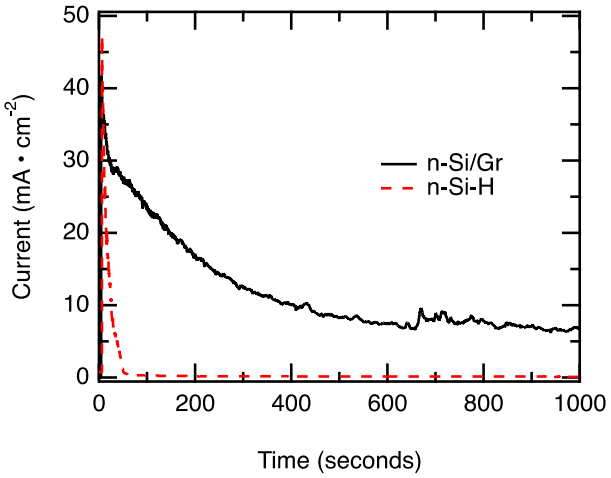

Figure S10. *J–t* behavior of an n-Si/Gr and a n-Si–H electrode in $Fe(CN)_6^{3-/4-}{}_{(aq)}$ under approximately ~100 mW cm^{-2} light intensity (ELH lamp) over 1000 s (E = 0 V vs. solution).

(1) Petrone, N.; Dean, C. R.; Meric, I.; van der Zande, A. M.; Huang, P. Y.; Wang, L.; Muller, D.; Shepard, K. L.; Hone, J. *Nano Letters* **2012**, *12*, 2751.

(2) The $NH_4(S_2O_8)_2$-etched n-Si/Gr electrodes demonstrated slightly larger fill factors than those derived from the $FeCl_3$ etch. However, the $NH_4(S_2O_8)_2$-etched n-Si/Gr electrodes also occasionally exhibited small parallel shunt resistances not indicative of typical photoelectrodes, such as those etched with $FeCl_3$ For these reasons, Figure 1 and Figure 3 report electrodes etched with $NH_4(S_2O_8)_2$ were used to obtain the data reported in Figure 1 and Figure 3 while electrodes etched with $FeCl_3$ were used to obtain the data reported in Figure 2.

(3) O'Leary, L. E.; Johansson, E.; Brunschwig, B. S.; Lewis, N. S. *The Journal of Physical Chemistry B* **2010**, *114*, 14298.

(4) Connelly, N. G.; Geiger, W. E. *Chemical Reviews* **1996**, *96*, 877.

(5) Ferrari, A. C.; Basko, D. M. *Nat Nano* **2013**, *8*, 235.

(6) Ni, Z.; Wang, Y. Y.; Yu, T.; Shen, Z. *Nano Res* **2008**, *1*, 273.

(7) Ponomarenko, L. A.; Yang, R.; Gorbachev, R. V.; Blake, P.; Mayorov, A. S.; Novoselov, K. S.; Katsnelson, M. I.; Geim, A. K. *Physical Review Letters* **2010**, *105*, 136801.

(8) Sze, S. M.; Ng, K., K. *Physics of Semiconductor Devices*; 3rd ed.; John Wiley & Sons, Inc.: Hoboken, NJ, 2007.

(9) Gerischer, H. *Physical Chemistry: An Advanced Treatise*; Academic Press: New York, 1970; Vol. IXA, Electrochemistry.

(10) Serpone, N.; Pelizzetti, E. *Photocatalysis: Fundamentals and Applications*; John Wiley & Sons, Inc.: Hoboken, NJ, 1989.

(11) Yan, R.; Zhang, Q.; Li, W.; Calizo, I.; Shen, T.; Richter, C. A.; Hight-Walker, A. R.; Liang, X.; Seabaugh, A.; Jena, D.; Xing, H. G.; Gundlach, D. J.; Nguyen, N. V. *Applied Physics Letters* **2012**, *101*, 022105.

(12) Bard, A. J.; Bocarsly, A. B.; Fan, F. R. F.; Walton, E. G.; Wrighton, M. S. *Journal of the American Chemical Society* **1980**, *102*, 3671.
(13) Bard, A. J.; Faulkner, L. R. *Electrochemical Methods: Fundamentals and Applications*; 2nd ed.; John Wiley & Sons, Inc.: Hoboken, NJ, 2001.
(14) Briggs, D.; Seah, M. P. *Practical Surface Analysis*; 2nd ed.; John Wiley & Sons Ltd, 1990.
(15) Hochella Jr, M. F.; Carim, A. H. *Surface Science* **1988**, *197*, L260.
(16) Haber, J. A.; Lewis, N. S. *The Journal of Physical Chemistry B* **2002**, *106*, 3639.